PCCP

PAPER

View Article Online
View Journal | View Issue

Cite this: *Phys. Chem. Chem. Phys.*, 2016, **18**, 4643

Band gap opening and semiconductor–metal phase transition in (*n*, *n*) single-walled carbon nanotubes with distinctive boron–nitrogen line defect†

Ming Qiu,[ab] Yuanyuan Xie,[a] Xianfeng Gao,[a] Jianyang Li,[a] Yelin Deng,[a] Dongsheng Guan,[a] Lulu Ma[a] and Chris Yuan*[a]

Received 9th November 2015,
Accepted 18th January 2016

DOI: 10.1039/c5cp06853c

www.rsc.org/pccp

Band gap opening and modulating are critical in dictating the functionalities of single walled carbon nanotubes (SWCNTs) in a broad array of nano-devices. Using first-principles density functional theory calculations, a class of semiconducting armchair SWCNTs with a distinctive BN line defect are studied, showing a super capacity to open the band gap of (4, 4) SWCNT to as large as 0.86 eV, while the opened band gap are found decreasing with the increasing diameters of SWCNTs. The opened band gap of SWCNTs can also be successfully modulated through both mechanical and electrical approaches by applying compressive uniaxial strain and electric field. This study provides novel insights into the large band gap opening and modulating of SWCNTs and could be useful in facilitating future applications of SWCNTs in electronic, optical and thermoelectric devices.

1 Introduction

With such superior properties as high carrier mobility, high thermal conductivity, high tensile strength, high Young's modulus and hollow structure *etc.*, single-walled carbon nanotubes (SWCNTs)[1,2] have found a wide range of applications on a number of functional devices including chemical sensors,[3,4] electrochemical devices,[5,6] hydrogen storage devices,[7,8] field emission devices[9,10] and nanoscale electronic devices,[11,12] *etc.* In general, these devices employ different material behaviors of SWCNTs ranging from metallic to semimetallic to semiconducting, as simply characterized by their increasing electronic band gap.[13,14] It was Deshpande *et al.*[15] who first found in their experiments that the metallic armchair SWCNTs have a band gap of 0.01–0.10 eV which could be potentially tuned to display different material properties from metallic to semiconducting on the same SWCNTs. This interesting finding has attracted enormous interests in recent years in opening the band gaps of metallic SWCNTs to obtain a tunable and applicable metallic-semiconducting molecular devices. To open the band gaps of metallic SWCNTs, two distinct strategies are typically adopted: internal or external feature approaches. The internal feature approach relies on modifying the SWCNT structure or inducing internal property change to open the band gap.[15–21] For example, with a corrugated structure, the band gaps of (3, 3) and (4, 4) SWCNTs could be opened to 0.280 and 0.095 eV, respectively;[16] with a phonon distortion, the band gap of a (3, 3) SWCNT can be opened to 0.25 eV;[17,18] with a bond rotation defect, the band gap of a (9, 0) zigzag SWCNT can be opened to about 0.50 eV,[19] and with a BN domain, the band gap of a (15, 0) zigzag SWCNT can be opened to 0.39 eV.[20] In contrast, the external feature approach takes advantages of external factors in opening the band gap of SWCNTs.[22–27] For instance, the tube–tube interactions in ropes of armchair SWCNTs can separate their conduction and valence bands by a gap of about 0.1 eV;[22–24] the vanadium atomic chain adsorbed on the outer surface of SWCNTs can strongly influence the electronic structure of the (6, 6) and (8, 8) metallic armchair SWCNTs and can open their band gaps to 0.49 eV;[25] a supporting silicon substrate under the SWCNTs has been found to be able to enlarge the band gap of a small armchair (3, 3) SWCNT to about 0.11 eV.[26,27]

After opening, the band gap of the SWCNT also needs to be continuously modulated to achieve precise phase transition between metallic and semiconducting properties which can greatly help to improve the device performance and expand its functionalities and applications.[28–31] For this purpose, a number of experimental techniques and theoretical methods have been developed in recent years. For instance, with metallofullerenes inserted, the SWCNTs can act as multiple quantum dots;[32] with bimolecular decoration, they can achieve metal–semiconductor

[a] *Department of Mechanical Engineering, University of Wisconsin Milwaukee, Wisconsin 53211, USA. E-mail: cyuan@uwm.edu*
[b] *School of Physics and Electronic Science, Changsha University of Science and Technology, Changsha 410114, China*

† Electronic supplementary information (ESI) available. See DOI: 10.1039/c5cp06853c

transition[33] and detect DNA hybridization[34] and conformational polymorphism;[35] with electrical,[36–38] mechanical[39,40] and magnetic approaches,[41] their band gaps can be modulated for potential applications in molecular devices. Among these available techniques, the mechanical and electrical approaches are most widely investigated, and the modulated devices are explored extensively as one of the most promising alternatives to the silicon-based electronic components. For mechanical modulating, a twisted armchair SWCNT has been found to show insulator-like conductivity through atomically resolved scanning tunneling microscopy images.[42] Mechanical squashing can lead to the conductance oscillations[43,44] and metal-to-semiconductor transition[45,46] in armchair SWCNT. For electrical modulating, the SWCNT shows a significantly increased current density (exceeding 10^9 A cm^{-2}),[47] Majorana bound states[48] and band gap modulation[49–51] under the electrical field as induced by dramatic scattering of electrons, proximity effect and axial polarization.

However, finding more CNT-based functional devices and tuning their characteristics to understand the fundamental physical mechanism and improve their performance are still remaining challenges. A particular question is whether a new class of CNTs can be constructed from graphene nanoribbons (GNRs), *via* Klein edges of GNRs.[52–56] He *et al.*[57] validated experimentally that the edges of GNRs can be transformed to form extended symmetric Klein edges which can be maintained stably for 2s before further structural transformation occurs. Meanwhile, the carbon atoms of the Klein defect can be replaced by groups,[58,59] metal[60] and non-metal atoms.[61–64] Interestingly, Šljivančanin[65] found the hydrogenated CNTs (5, 5) have similar properties with 10-zigzag GNR (ZGNR). Lee *et al.*[66] investigated the half metallicity of hydrogenated CNT (8, 8) and found it is similar with 16-ZGNR.[67] Du *et al.*[14] fabricated BNC nanotubes from the BN and C domains. The above results illustrate that it is possible to roll up the edge-modified GNRs to build a new class of SWCNTs which could pave a new way to extend the families of carbon-based materials and demonstrate more interesting functionality and applicability for future molecular devices.

Obviously, connecting the two modified edges of GNR can introduce certain domains. These defects can break the structural symmetry and change the electronic structures which could help open the band gap of new built CNTs. While significant efforts have been made recently on band gap opening and continuous modulating of SWCNTs, the best result reported in literature on band gap opening of SWCNTs is only 0.50 eV.[19] In this paper, we predict a new class of semiconducting armchair SWCNT and successfully obtained a large band gap opening with a distinctive BN line defect, using both mechanical and electrical modulating for a precise control of the semiconductor–metal phase transition. We also propose a new method to break the structural symmetry of the armchair SWCNT which the dipole moments induced by the BN defect can take the key place to enhance the device performance. First-principles density functional theory (DFT) is used for the simulation. The fundamental mechanism for the large band gap opening and modulating are explained and reported in details.

2 Methods and structures

In this study, first-principles DFT is employed to calculate the band gap opening and modulating of armchair SWCNT, based on a supercell configuration using the Atomistix Toolkit (ATK).[68,69] As shown in Fig. 1, the armchair SWCNT with BN line defect is constructed from a zigzag graphene nanoribbon (ZGNR) with B and N terminations each on one side which also can be understood as the heterostructure consisting of BN single-walled nanotube[70–72] and graphene. In the calculation, the generalized gradient approximation (GGA) within Perdew–Burke–Ernzerhof (PBE) form[73] is used as the exchange–correlation function. It has been reported that DFT-PBE calculations can underestimate the band gaps of many materials, but for CNTs, graphene and BNC nanostructures, it can describe the band structure and trend properly and correctly.[74–76] Norm-conserving pseudo-potentials are employed to represent the atomic core and double ζ plus double polarization basis sets to expand the valence states of electrons. In the calculation, the mesh cutoff is set at 200 Hartree, with a $1 \times 1 \times 33$ *K*-point grid. In the supercell configuration, a sufficiently large separation (about 20 Å) between adjacent SWCNTs and ZGNRs is maintained. In order to minimize the perturbation from the internal force and to better understand the ground state properties, the geometries of the supercells, including the ZGNRs and SWCNTs, are optimized through Quasi-Newton method until all residual forces on each atom are smaller

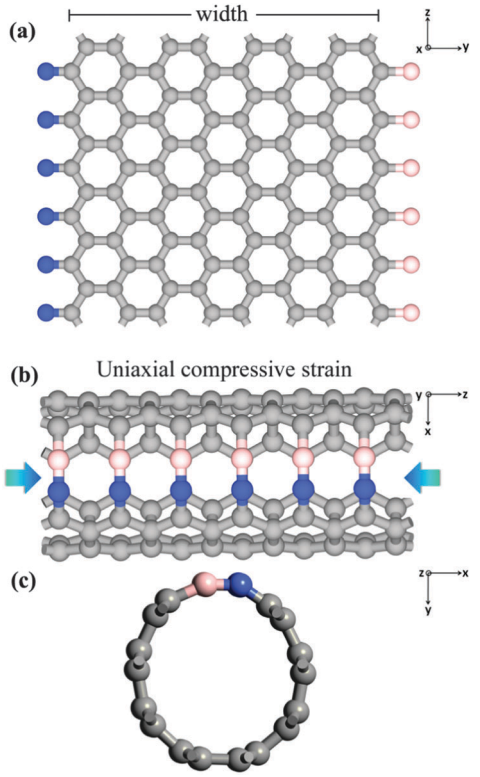

Fig. 1 (a) Model geometry of (4, 4) ZGNR terminated with Boron (color pink) and Nitrogen (color blue) atoms each on one side. (b) Model geometry of (4, 4) armchair SWCNT with B–N line defect. (c) The side-view of (4, 4) armchair SWCNT with B–N line defect.

than 0.005 eV Å^{-1} and the maximum stress along the z direction of the supercell is smaller than 0.005 eV Å^{-3}.

In the DFT calculations, the formation energy denoting the energy transfer from bn@ZGNR to bn@CNT, is calculated through:

$$E_{\text{form}} = E_{\text{bn@CNT}} - E_{\text{bn@ZGNR}} \quad (1)$$

where $E_{\text{bn@CNT}}$ and $E_{\text{bn@ZGNR}}$ are the total energies of the bn@CNT and bn@ZGNR, respectively. The bn@ZGNR is the zigzag graphene nanoribbon with B and N terminations each on one edge. The bn@CNT, as studied, is the BNC heterostructure fabricated from the bn@ZGNR. The density of states describing the states distributions at each energy level available to be occupied, is calculated through:

$$D(\varepsilon) = \frac{1}{N_k}\sum_k \delta[\varepsilon - E_n(k)] \quad (2)$$

where N_k is the total number of K points in the first Brillouin zone, k is the wave vector in the reciprocal space and $E_n(k)$ is the energy eigenvalue that forms the energy bandstructure. The molecular projected self-consistent Hamiltonian (MPSH) of the eigenvalue $E_n(k)$, obtained by diagonalizing its self-consistent Hamiltonian, is considered as the renormalization of the molecular orbital and depicted as the state wave-function distributions in the real space. In the calculation, MPSH is defined as:

$$\Psi_{n,k}(r) = \sum_{\mu\nu} \varphi_\mu(r)\Psi_{n,\mu\nu}(k)\varphi_\nu^*(r) \quad (3)$$

where $\varphi_\mu(r)$ and $\varphi_\nu(r)$ are the basis of atomic orbitals μ and ν, and $\Psi_{n,\mu\nu}(k)$ is the corresponding wavefunction with:

$$H_{\mu\nu}(k)\Psi_{n,\mu\nu}(k) = E_n(k)S_{\mu\nu}\Psi_{n,\mu\nu}(k) \quad (4)$$

Here, $S_{\mu\nu}$ is the overlap matrix. The effective mass of carriers is defined as:

$$m^* = \hbar^2[\mathrm{d}^2E_n(k)/\mathrm{d}k^2]^{-1} \quad (5)$$

where $\hbar$ is the reduced Planck constant. The carriers velocity with the group velocity of the wave package is defined as:

$$v_g = P/m^* = \hbar k/m^* \quad (6)$$

where P is the momentum.

Development of such armchair SWCNTs with a distinctive BN line defect is possible from experimental perspective. Previous experimental results have shown that the atomic layers of h-BNC[71] and BNC nanotubes[77] can be deposited on the Cu and Ni–Fe-coated SiO_2/Si substrates. The BN and C domains show energetically stable to form the heterostuctures.[14] Similarly, the graphene nanostructure terminated with B or N has been reported.[64] Accordingly, like the reported work,[14,65,66] it is possible to construct new GNR and SWCNT with metal or non-metal line defects. To validate this idea, we first build two ZGNRs that one is terminated with B and H each on one side, and the other has N and H terminations each on one side. Using CASTEP, we reduce the distance of B and N sides of two ZGNRs and perform a molecular dynamics simulation. The molecular dynamics results show that the two ZGNRs can be connected to form a new ZGNR with BN line defect. Then, we construct a ZGNR with B and N each on one side and wrap this ZGNR to reduce the distance of B and N to about 3.7 Å (about corresponding B and N atoms can bond side-to-side to form a 3 times of the length of BN bond). The results show that the corresponding B and N atoms can bond side-to-side to form a new BNC hetero-structure, bn@CNT (Mov. S1, ESI†), to finally obtain the SWCNT with BN line defect.

As shown in Fig. 1(a) and (b), a (4, 4) bn@CNT was fabricated following above procedure using the (4, 4) bn@ZGNR whose corresponding B and N atoms were side-to-side connected to form the distinctive B–N line defect. The new (4, 4) bn@CNT is referred to as 4bn@CNT. In the formula, the number 4 represents the width of bn@ZGNR from which the 4bn@CNT is fabricated. After the BN line defect being developed, the structural symmetry of the SWCNT has been changed, so in this paper the width of bn@ZGNR is used to represent the diameter of corresponding bn@CNT. In this heterostructure, N has an electronegativity[78] larger than B and C, χ(N) = 3.04 > χ(C) = 2.55 > χ(B) = 2.04; therefore, electrons can move from B to C and to N. For B- or N-terminated ZGNRs, the N-terminated edge-states are charged with transferred electrons from neighboring C atoms, while B-terminated edge-states are creating holes by losing electrons to neighboring C atoms. Then, the edge-states of ZGNRs with B- or N-terminated are delocalized,[64,79] and the ZGNRs with B and N attached on each edge are strongly metallic (Fig. S1, ESI†) because of the asymmetrical delocalized edge-states on each side.

3 Results and discussion

3.1 Gap opening

The evolution in band gap energy of bn@CNTs with different widths from 4 to 24 is calculated and presented in Fig. 2; the inset is the dipole moment of bn@CNTs along the z axis with widths from 4 to 24. The width-dependent formation energy indicates that it is an exothermic fabrication process from bn@ZGNR to bn@CNT, and the formation energy is found decreasing with the increasing width, as shown in Fig. S2 (ESI†). The results in Fig. 2 illustrates that the band gap of SWCNTs has been opened obviously, while the opened gap decreases with the increasing width. As shown in Fig. 2, the DFT calculated band gap opening of bn@CNTs with widths of 4, 8, 12, 16, 20 and 24 are 0.86, 0.60, 0.46, 0.35, 0.27 and 0.24 eV, respectively. To the best of our knowledge, the band gap opening of small CNT (*i.e.* 4bn@CNT) to 0.86 eV, is the largest gap opening ever reported in literature.

The first reason for this large band gap opening is the different bond energies which separates the bn@CNT into two domains: the BC_2N (the BN and their first neighboring carbon atoms) and C (other carbon atoms) domains. On bn@CNT, the calculated average lengths of B–C, B–N and C–N bonds are 1.49, 1.29 and 1.33 Å, respectively, which are shorter than those (1.52, 1.45 and 1.39 Å, respectively) of the single layer of h-BNC.[80] With an inverse relationship between bond length and bond energy,

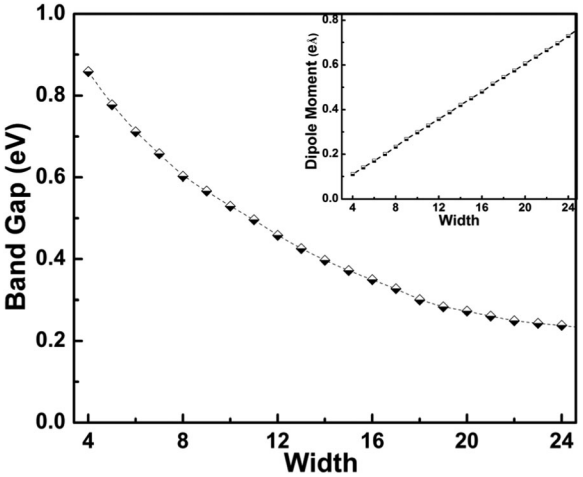

Fig. 2 The evolution in band gap energy of bn@CNTs with different widths from 4 to 24. The inset is the dipole moment along the *z* axis with the widths from 4 to 24.

the B–C, B–N and C–N bonds show higher bond energies than those on the single layer of h-BNC. Especially for the B–N bond, the bond length is reduced more than 11%. Due to the ionic nature, it undoubtedly has higher bond energy and can enhance the tendency to segregate the BC_2N and C domains. From the Mülliken population analysis, although the B (N) on the bn@CNTs donates (accepts) about 150% more electrons than the B (N) on the bn@ZGNRs, the BN line defect contributes about 0.02*e* to the neighboring carbon atoms. Simply, the N and neighboring C atoms take most of B's p electrons away. That is why its electron density (Fig. S3, ESI†) changes and affects the transport eigen-channels on the bn@CNT.

The second reason for the large band gap opening is that the structural mirror asymmetry of bn@CNT, as induced by the BN line defect, not only leads to two different domains, but also introduces three permanent dipole moments. First, the charge asymmetry distribution on the BN line defect has a local dipole moment (along the *x* axis), and the two asymmetric hybridized states on the two C atoms of B–C and N–C bonds form a small dipole moments counteract with each other and reduce the total dipole moment reversed to the B–N direction. But these two dipole moment along the *x* axis. Second, the BC_2N domain forms a coulomb dipole moment (along the *y* axis) with the carbon atoms on the cross-section ring. But from our Mülliken population analysis, the BN line defect denotes only a little charge (about 0.02*e*) to the C carbon atoms which does not contribute much to the gap opening. Third, the BN line defect yields a bond dipole moment along the *z* axis which is induced jointly by the hybridization and asymmetrical distribution of BN states. Based on our calculations, the BN bond in the bn@CNT is shortened with the increasing of width (Fig. S4, ESI†). The shortened BN bond enhances the hybridization of BN states, and directly induces the increasing of the bond dipole moment with width along the *z* axis (Fig. 2). With such moments, the structural symmetry of pristine SWCNT is broken, and a gap is then opened and π–π^* hybridization follows.

As calculated, the bn@CNTs gap opening decrease from 0.86 eV to 0.24 eV with the increasing width from 4 to 24. The results are shown in Fig. 2, which is in good agreement with the linear dependence of the effective mass and tube diameter as reported before.[81] The calculated band structures of bn@CNTs with different widths of 4, 8, 12 and 16 are presented in Fig. 3. From this figure, the opened bn@CNTs with small widths 4 and 8, are indirect band gap semiconductors with the highest occupied molecular orbital (HOMO) located at Γ point and lowest unoccupied molecular orbital (LUMO) located at *K* point. This clearly indicates that the BN line defect has significant effect on breaking the symmetry of small bn@CNTs. With the increasing of the bn@CNT diameter, the shortened B–N bond (Fig. S4, ESI†) increases the hybridization of the BN line defect and dipole moments along the *z* axis. The opened large bn@CNTs with widths 12 and 16 become direct band gap semiconductors with HOMO and LUMO both located at *K* point. When the tube diameter approaches infinity, the band structure of bn@CNT is close to that of pristine armchair SWCNTs added with BN states which is the band structure located near the Γ point. From the projected density of states (Fig. S5, ESI†), the HOMO consists of three states (B, C and N atoms), while the LUMO is mostly built on C atoms. Combined with the band structure, the density of states of valance band consists of two parts: the states near the Γ point distributing mostly on the BN line defect (more on N atom) and the states near the Dirac point spreading on the C atoms. The conduction band consists of states on the carbon atoms. From our calculation, the states of the conduction band mostly come from the C atoms near the B atom. The valance band is consisting of 2p orbitals of C and 2p hybrid states of BN, while the conduction band is mostly composed of the states on C atoms. For large width bn@CNTs, the states of 2p orbital of C atoms take more weight and come closer to the Fermi level than the hybrid states of BN. As a result, the bn@CNT becomes the direct band gap.

3.2 Mechanical modulating of opened band gaps

In this section, the mechanical modulating of opened band gap is simulated under uniaxial compressive strain, as shown in

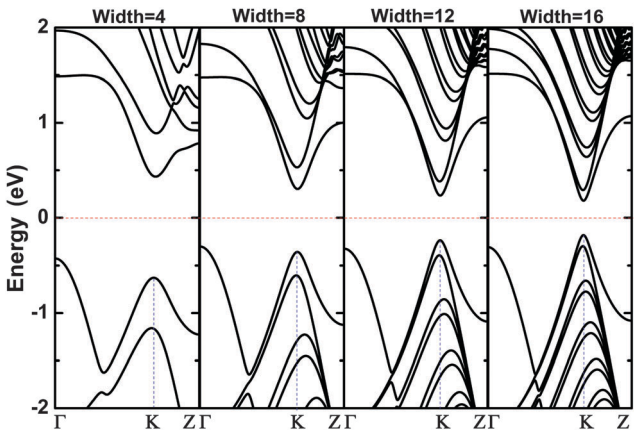

Fig. 3 The band structures of bn@CNTs with different widths 4, 8, 12 and 16.

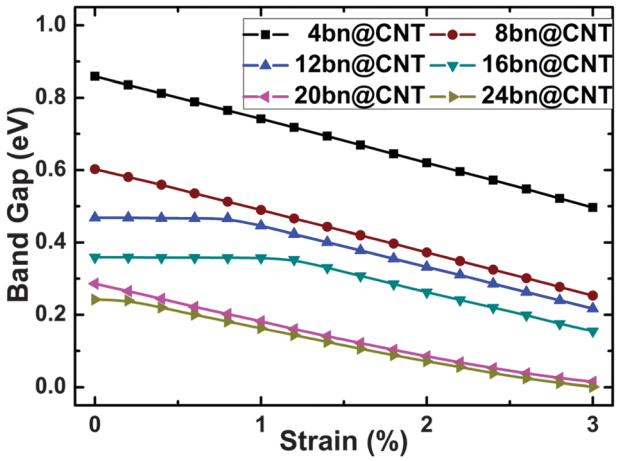

Fig. 4 The variation in band gaps of bn@CNTs with different widths 4, 8, 12, 16, 20 and 24 under the uniaxial compressive strain.

Fig. 4 for different widths 4, 8, 12, 16, 20 and 24. The applied compressive strain is in the range of 0–3% of the *z*-axis lattice length. From Fig. 4, the electronic structure of bn@CNT is found sensitive to the uniaxial compressive deformation. The band gaps of all studied bn@CNTs decrease in a linear relationship with increasing compressive strain except the 12bn@CNT and 16bn@CNT, which change slightly during 0–1% strain level. From the results, applying 3% compressive strain can reduce the band gap of 4bn@CNT from 0.86 eV to 0.49 eV, while reduce the band gap of 20bn@CNT from 0.27 eV to 0.01 eV. For the 12bn@CNT and 16bn@CNT, the band gaps begin to decrease rapidly from 0.8% and 1.2% strain, respectively. In summary, the 3% compressive strain can transfer the 20bn@CNT and 24bn@CNT from semiconductor to metal; with the increasing of the compressive strain, the 4bn@CNT, 8bn@CNT, 12bn@CNT and 16bn@CNT will undergo certain phase transitions as well.

The band structures of 4bn@CNT and 12bn@CNT under different uniaxial compressive strains are calculated and presented in Fig. 5. As known from the simple bond rule, B–N bonds are stronger than the B–C and C–N bonds. When the uniaxial compressive strain is applied, the B–C and C–N bonds are lengthened while the B–N bond and first C–C bonds adjacent to the B–C and C–N bonds on the bn@CNT are gradually shortened. Electrons transferred from B atom to its neighboring N and C atoms are accordingly reduced. As a result, the dipole moment along the *y* axis decreases (Fig. S6, ESI†), while the dipole moments along the *x* and *z* axes increase slightly. In this way, the charges are redistributed, and the effect of the dipole moment on the polarization is reduced. From Fig. 5(a) and (b), this redistribution also leads to the moving of the HOMO and LUMO close to the Fermi level, as the strain increases (Fig. S7, ESI†). From the calculations, the chemical potential shifts up-ward with the increasing of strain. For 12bn@CNT and 16bn@CNT, they have direct band gaps in the ground state. However, under the compressive deformation, the states on the Γ point, mostly composed of the states on the BN line defect (Fig. S8, ESI†), shift faster up-ward to

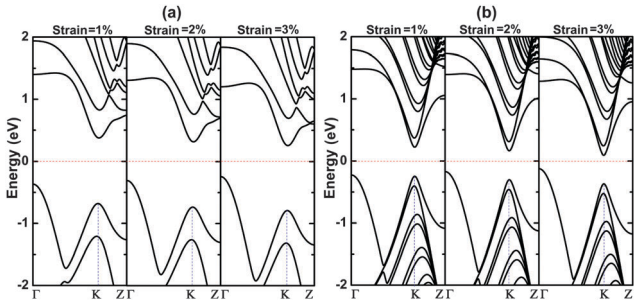

Fig. 5 The band structures of (a) 4bn@CNT and (b) 12bn@CNT under different uniaxial compressive strain.

approach the Fermi level than that on the *K* point. With the increasing strain, they pass the states on the *K* point and change the gaps of 12bn@CNT and 16bn@CNT from direct to indirect band gaps. In this way, the different sensitivity of states and the continuous change of bond length, charge redistribution and dipole moment all contribute to the mechanical modulating of the opened band gap.

For comparison, the electronic properties of the bn@CNTs under uniaxial elastic strain is also calculated and it is found that, under 5% elastic strain, the band gaps are widened 26.5%, 11.9%, 2.4% and 1.1% for 4bn@CNT, 8bn@CNT, 12bn@CNT and 16bn@CNT, respectively. Interestingly, the band structures show that the bn@CNTs are semiconductors with direct band gaps under elastic strain, which indicates that the states on the *K* point are more sensitive to elastic strain than those on the Γ point. This means the BN line defect is more sensitive to the compressive strain, while the C atoms are more sensitive to the elastic strain.

For device application, the evolution of effective electron mass (in units of the free electron mass m_e) with different widths under the compressive strain is calculated and presented in Fig. 6. The width- and strain-dependent effective electron mass is found decreasing linearly with uniaxial compressive strain. Nevertheless, the decreasing trend is diminishing with the increasing of widths from 4 to 24. From the results, the effective electron mass of

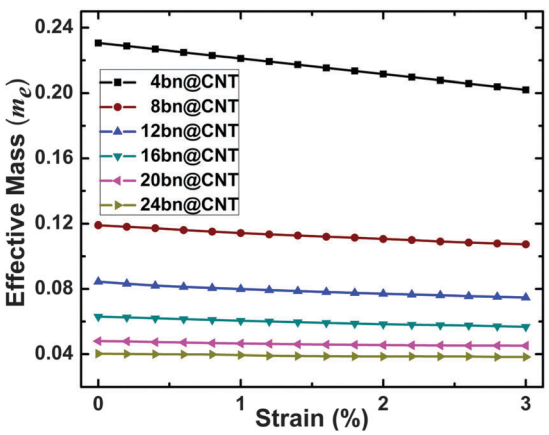

Fig. 6 The evolutions of effective electron mass (in units of the free electron mass m_e) with different widths under uniaxial compressive strain.

4bn@CNT, 12bn@CNT and 20bn@CNT decreases by 12%, 11% and 6% from 0.230 m_e to 0.202 m_e, 0.084 m_e to 0.075 m_e, and 0.048 m_e to 0.045 m_e respectively, under 3% uniaxial compressive strain. Because of the inverse relationship between mass and velocity, it shows that the carrier mobility of bn@CNT can be effectively tuned by uniaxial compressive deformation.

3.3 Electrical modulating of opened band gaps

In this section, the electrical modulating of opened band gap is computed between −0.10 to +0.10 V Å^{-1}. The modulated band gap results are calculated and presented in Fig. 7. Our DFT calculations indicate that the large bn@CNTs are more sensitive to the applied electric field modulating. Fig. 7 shows the modulated band gaps for different widths 16, 20 and 24. From this figure, the band gaps of large bn@CNTs can be effectively modulated by both positive and negative electric field applied along the y axis. Benchmarking between the three different widths of opened bn@CNTs, the 24@CNT is most sensitive to the applied electric field and is the most quickly approaching metallic under the same electric field. Under a electric field of −0.10 (0.10) V Å^{-1}, the band gap of 16bn@CNT decreases from 0.36 to 0.02 (0.05) eV, while for 24bn@CNT, a small field of −0.04 (0.04) V Å^{-1} can reduce its band gap from 0.24 to 0.02 (0.03) eV. Nevertheless, those small diameter bn@CNTs are slightly resistive to the applied electric field. Our calculated results show that the band gaps of 4bn@CNT and 8bn@CNT will decrease. For comparison, the electrical modulating of band gaps of bn@CNTs under electric field applied along the x axis are also calculated and shown in Fig. S9 (ESI†). They all have similar switching behaviors, while the modulating is more sensitive to the electric field applied along the y axis.

As an example, the 16bn@CNT is used to explain the field-effect behavior under the electrical modulating, and the modulated band structures under electric fields applied along the y axis are shown in Fig. 8. From this figure, the band gap decreases quickly with the increasing of electric field. From the electric fields of 0.05 (−0.05) to 0.10 (−0.10) V Å^{-1}, the states near the minimum of conduction band (maximum of valance band) show a degeneracy of the states, and the states on the Γ point shift up (down) slightly. The positive

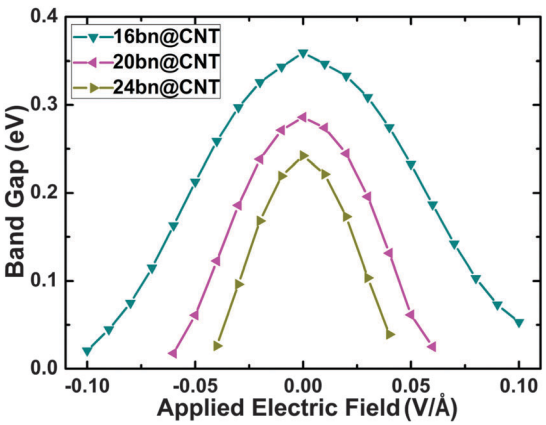

Fig. 7 The variation in band gaps of bn@CNTs with different widths 16, 20 and 24 under electric field applied along the y axis.

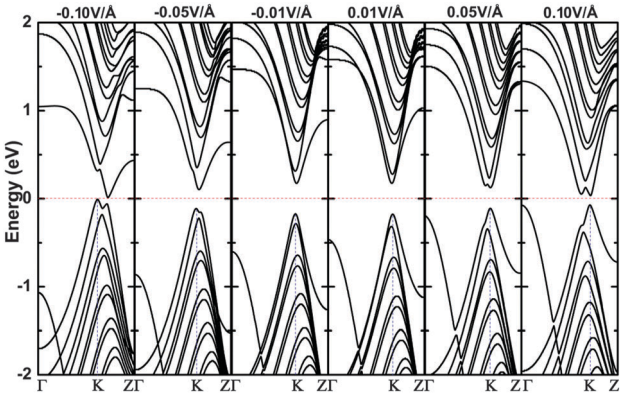

Fig. 8 The band structures of 16bn@CNT under different electric fields along the y axis.

applied electric field keeps the direct band gaps of 16bn@CNT, while the negative electric field switches it to indirect band gaps. From the figure, the LUMO moves away from the Fermi level only at an electric field of 0.01 and 0.02 V Å^{-1}. Then, the LUMO shifts downward and is moving closer to the Fermi level at an electric field of −0.10 V Å^{-1} than that at 0.10 V Å^{-1}. The HOMO shifts upward to the Fermi level, while it moves faster under the positive electric field. For further investigation, the eigenstates from the MPSH calculations at the electric fields of 0, ±0.01 and ±0.10 V Å^{-1} are shown in Fig. S10 (ESI†). The HOMOs always locate at the BN line defect and partially at the C atom neighboring N atom. The LUMO distributes mostly on the top area, at the BN line defect and their neighboring C atoms under the negative and low positive electric field (0.01 V Å^{-1}). But under an electric field of 0.10 V Å^{-1}, the LUMO locates on the bottom area. From our projected density of states calculation, the states near the Fermi level are mostly composed of the 2p orbitals of BN line defect and their neighboring C atoms (the C atoms near the bottom) under a gate voltage of −0.10 (0.10) V Å^{-1}, which also agrees well with our calculated MPSH results as described above. As found, the increasing electric fields change the effective work functions and decrease the HOMO–LUMO gap of 16bn@CNT. From Fig. 8, the degenerate states shift towards the Fermi level and split to nondegenerate under high applied voltages induced by the increase of the coulomb repulsion near the Fermi level.

To further investigate the modulating behavior, the evolutions of dipole moments for different widths 16, 20 and 24 bn@CNTs under the −0.10 to +0.10 V Å^{-1} applied along the y axis, which take the most weight, are calculated and shown in Fig. 9. With the increasing electric field, the B atom keeps accepting the charge transferring from its neighboring C and N atoms while the N atom keeps donating the charge to its neighboring B and C atoms. This charge redistribution on the BC_2N domain increases (decreases) the dipole moment along the x (z) axis. The BN line defect keeps denoting more charges to the carbon atoms with the increasing of applied electric field which leads to the linearly decreasing of the dipole moment along the y axis.

As an example, the evolution of the effective electron and hole mass (in units of the free electron mass m_e) of the 16bn@CNT

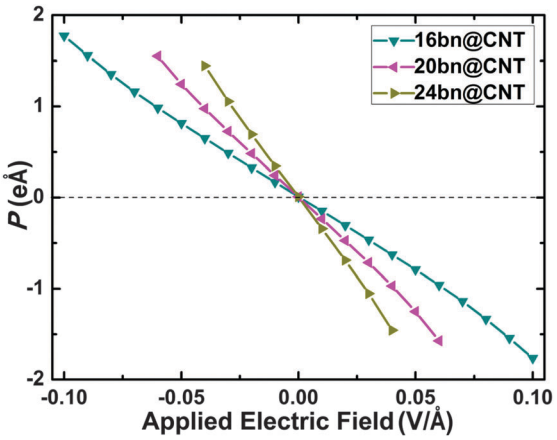

Fig. 9 The evolutions of dipole moments with different widths 16, 20 and 24 under the electric field applied along the *y* axis.

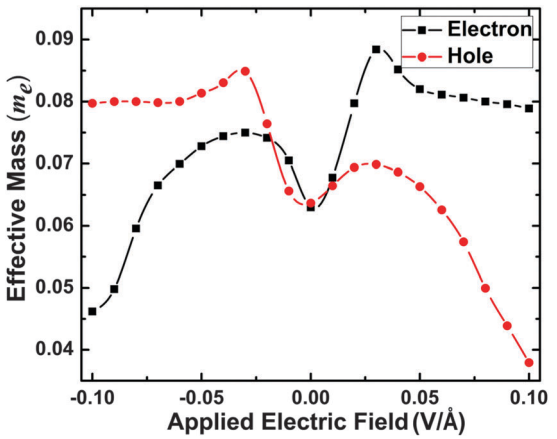

Fig. 10 The evolutions of effective electron and hole mass (in units of the free electron mass m_e) of 16bn@CNT under different electric field applied along the *y* axis.

under the −0.10 to +0.10 V Å^{-1} is calculated and presented in Fig. 10. From this calculation, the effective electron and hole mass increase from the ground state to the electric fields of −0.03 and +0.03 V Å^{-1} and decrease below −0.03 V Å^{-1} and above +0.03 V Å^{-1}. As a small effective mass reflects a high mobility and conductivity, the Fig. 10 results show that under low (−0.10 V Å^{-1}) and high (+0.10 V Å^{-1}) electric fields, the 16bn@CNT demonstrates a metallic behavior. With an increasing negative (positive) electric field applied, the effective electron (hole) mass decreases obviously, while the effective hole (electron) mass reduces slightly. It illustrates the electron (hole) plays the most important role in electron transport under the negative (positive) gates, and the carrier mobility and electronic structure of 16bn@CNT can be effectively modulated by the applied electric field.

4 Conclusions

Using first-principles density functional theory calculations, we investigated the band gap opening and modulating of a new class of semiconducting armchair SWCNT with a BN line defect. It is found that the BN line defect not only breaks the structural symmetry of the armchair SWCNT, but also induces shorter BN bond with higher bond energy and three permanent dipole moments to enhance the band gap opening, while the dipole moment along the *z* axis plays the most important role. The calculated results show that the gap opening of bn@CNTs with widths of 4, 8, 12, 16, 20 and 24 are 0.86, 0.60, 0.46, 0.35, 0.27 and 0.24 eV, respectively. The 0.86 eV gap opening of small bn@CNT (*i.e.* 4bn@CNT) is the largest gap opening ever reported in literature.

The band gaps of bn@CNT are modulated using both mechanical and electrical approaches to achieve semiconductor–metal phase transitions. For mechanical modulating, uniaxial compressive strain in the range of 0–3% of the *z*-axis lattice length are applied for different widths of 4, 8, 12, 16, 20 and 24. It is found the band gaps of most studied bn@CNTs decrease in a linear relationship with increasing compressive strain except the 12bn@CNT and 16bn@CNT, which change slightly during 0–1% strain level. It is also found that applying 3% compressive strain can reduce the band gap of 4bn@CNT from 0.86 eV to 0.49 eV, and 20bn@CNT from 0.27 eV to 0.01 eV. For electrical modulating, the opened band gap is computed between −0.10 to +0.10 V Å^{-1} electric fields. As found from the study, those large bn@CNTs are more sensitive to the electric field modulating, *i.e.*, for 24bn@CNT, a small voltage of −0.04 (0.04) V Å^{-1} can reduce their band gaps from 0.24 to 0.02 (0.03) eV; while those small bn@CNTs are slightly resistive to the electric field applied, *i.e.*, the band gaps of 4bn@CNT and 8bn@CNT decrease to 98% (90%) and 90% (70%) under −0.10 (0.10) V Å^{-1}.

Acknowledgements

The work described in this paper was fully supported by grants from the University of Wisconsin Milwaukee Research Growth Initiative grant program and the China National Natural Science Foundation (Grant No. 51302022).

References

1 S. Iijima and T. Ichihashi, *Nature*, 1993, **363**, 603.
2 R. H. Baughman, A. A. Zakhidov and W. A. de Heer, *Science*, 2002, **297**, 787.
3 P. G. Collins, K. Bradley, M. Lshigami and A. Zettl, *Science*, 2000, **287**, 1801.
4 J. Wang, M. Musameh and Y. Lin, *J. Am. Chem. Soc.*, 2003, **125**, 2408.
5 K. H. An, W. S. Kim, Y. S. Park, J. M. Moon, D. J. Bae, S. C. Lim, Y. S. Lee and Y. H. Lee, *Adv. Funct. Mater.*, 2001, **11**, 387.
6 M. Kaempgen, C. K. Chan, J. Ma, Y. Cui and G. Gruner, *Nano Lett.*, 2009, **9**, 1872.
7 A. C. Dillon, K. M. Jones, T. A. Bekkedahl, C. H. Kiang, D. S. Bethune and M. J. Heben, *Nature*, 1997, **386**, 377.
8 C. Liu, Y. Y. Fan, M. Liu, H. T. Cong, H. M. Cheng and M. S. Dresselhaus, *Science*, 1999, **286**, 1127.

9 S. S. Fan, M. G. Chapline, N. R. Franklin, T. W. Tombler, A. M. Cassell and H. J. Dai, *Science*, 1999, **283**, 512.
10 K. Jensen, J. Weldon, H. Garcia and A. Zettl, *Nano Lett.*, 2007, **7**, 3508.
11 Z. Yao, C. L. Kane and C. Dekker, *Phys. Rev. Lett.*, 2000, **84**, 2941.
12 J. Nygard, D. H. Cobden and P. E. Lindelof, *Nature*, 2000, **408**, 342.
13 J. W. G. Wilder, L. C. Venema, A. G. Rinzler, R. E. Smalley and C. Dekker, *Nature*, 1998, **391**, 59.
14 A. J. Du, Y. Chen, Z. H. Zhu, G. Q. Lu and S. C. Smith, *J. Am. Chem. Soc.*, 2009, **131**, 1682.
15 V. V. Deshpande, B. Chandra, R. Caldwell, D. S. Novikov, J. Hone and M. Bockrath, *Science*, 2009, **323**, 106.
16 H. X. Lu, J. B. Wu and W. Y. Zhang, *Phys. Rev. B: Condens. Matter Mater. Phys.*, 2013, **88**, 035423.
17 D. Connétable, G. M. Rignanese, J. C. Charlier and X. Blase, *Phys. Rev. Lett.*, 2005, **94**, 015503.
18 G. Dumont, P. Boulanger, M. Côté and M. Ernzerhof, *Phys. Rev. B: Condens. Matter Mater. Phys.*, 2010, **82**, 035419.
19 V. H. Crespi, M. L. Cohen and A. Rubio, *Phys. Rev. Lett.*, 1997, **79**, 2093.
20 V. V. Ivanovskaya, A. Zobelli, O. Stéphan, P. R. Briddon and C. Colliex, *J. Phys. Chem. C*, 2009, **113**, 16603.
21 A. Kleiner and S. Eggert, *Phys. Rev. B: Condens. Matter Mater. Phys.*, 2001, **63**, 073408.
22 P. Delaney, H. J. Choi, J. Ihm, S. G. Louie and M. L. Cohen, *Nature*, 1998, **391**, 466.
23 P. Delaney, H. J. Choi, J. Ihm, S. G. Louie and M. L. Cohen, *Phys. Rev. B: Condens. Matter Mater. Phys.*, 1999, **60**, 7899.
24 M. Ouyang, J. L. Huang, C. L. Cheung and C. M. Lieber, *Science*, 2001, **292**, 702.
25 C. K. Yang, J. J. Zhao and J. P. Lu, *Nano Lett.*, 2004, **4**, 561.
26 J. Y. Lee and J. H. Cho, *Appl. Phys. Lett.*, 2006, **89**, 023124.
27 M. R. Amer, A. Bushmaker and S. B. Cronin, *Nano Lett.*, 2012, **12**, 4843.
28 X. Y. Zhao, C. M. Wei, L. Yang and M. Y. Chou, *Phys. Rev. Lett.*, 2004, **92**, 236805.
29 Z. G. Wu, J. B. Neaton and J. C. Grossman, *Phys. Rev. Lett.*, 2008, **100**, 246804.
30 S. Mandal. and R. Pati, *Chem. Phys. Lett.*, 2009, **479**, 244.
31 J. A. Brehm, S. M. Young, F. Zheng and A. M. Rappe, *J. Appl. Phys.*, 2013, **114**, 224304.
32 J. Lee, H. Kim, S. J. Kahng, G. Kim, Y. W. Son, J. Ihm, H. Kato, Z. W. Wang, T. Okazaki, H. Shinohara and Y. Kuk, *Nature*, 2002, **415**, 1005.
33 M. Cha, S. Jung, M. H. Cha, G. Kim, J. Ihm and J. Lee, *Nano Lett.*, 2009, **9**, 1345.
34 E. S. Jeng, A. E. Moll, A. C. Roy, J. B. Gastala and M. S. Strano, *Nano Lett.*, 2006, **6**, 371.
35 D. A. Heller, E. S. Jeng, T. K. Yeung, B. M. Martinez, A. E. Moll, J. B. Gastala and M. S. Strano, *Science*, 2006, **311**, 508.
36 D. S. Novikov and L. S. Levitov, *Phys. Rev. Lett.*, 2006, **96**, 036402.
37 S. J. Tans, A. R. M. Verschueren and C. Dekker, *Nature*, 1998, **393**, 49.
38 R. Martel, T. Schmidt, H. R. Shea, T. Hertel and Ph. Avouris, *Appl. Phys. Lett.*, 1998, **73**, 2447.
39 C. L. Kane and E. J. Mele, *Phys. Rev. Lett.*, 1997, **78**, 1932.
40 L. Yang and J. Han, *Phys. Rev. Lett.*, 2000, **85**, 154.
41 U. C. Coskun, T. C. Wei, S. Vishveshwara, P. M. Goldbart and A. Bezryadin, *Science*, 2004, **304**, 1132.
42 W. Clauss, D. J. Bergeron and A. T. Johnson, *Phys. Rev. B: Condens. Matter Mater. Phys.*, 1998, **58**, R4266.
43 T. W. Tombler, C. W. Zhou, L. Alexseyev, J. Kong, H. J. Dai, L. Liu, C. S. Jayanthi, M. J. Tang and S. Y. Wu, *Nature*, 2000, **405**, 769.
44 C. Gómez-Navarro, J. J. Sáenz and J. Gómez-Herrero, *Phys. Rev. Lett.*, 2006, **96**, 076803.
45 J. Q. Lu, J. Wu, W. H. Duan, F. Liu, B. F. Zhu and B. L. Gu, *Phys. Rev. Lett.*, 2003, **90**, 156601.
46 C. J. Park, Y. H. Kim and K. J. Chang, *Phys. Rev. B: Condens. Matter Mater. Phys.*, 1999, **60**, 10656.
47 Z. Yao, C. L. Kane and C. Dekker, *Phys. Rev. Lett.*, 2000, **84**, 2941.
48 J. Klinovaja, S. Gangadharaiah and D. Loss, *Phys. Rev. Lett.*, 2012, **108**, 196804.
49 J. O'Keeffe, C. Y. Wei and K. Cho, *Appl. Phys. Lett.*, 2002, **80**, 676.
50 Y. Li, S. V. Rotkin and U. Ravaioli, *Nano Lett.*, 2003, **3**, 183.
51 F. Xu, M. Y. Wu, N. S. Safron, S. S. Roy, R. M. Jacobberger, D. J. Bindl, J. H. Seo, T. H. Chan, Z. Q. Ma and M. S. Arnold, *Nano Lett.*, 2014, **14**, 682.
52 P. Koskinen, S. Malola and H. Häkkinen, *Phys. Rev. B: Condens. Matter Mater. Phys.*, 2009, **80**, 073401.
53 A. Cresti and S. Roche, *Phys. Rev. B: Condens. Matter Mater. Phys.*, 2009, **79**, 233404.
54 Z. Liu, K. Suenaga, P. J. F. Harris and S. Iijima, *Phys. Rev. Lett.*, 2009, **102**, 015501.
55 K. Suenaga and M. Koshino, *Nature*, 2010, **468**, 1088.
56 J. S. Kim, J. H. Warner, A. W. Robertson and A. I. Kirkland, *ACS Nano*, 2015, **9**, 8916.
57 K. He, A. W. Robertson, S. Lee, E. Yoon, G. D. Lee and J. H. Warner, *Nano Lett.*, 2014, **8**, 12272.
58 O. Hod, V. Barone, J. E. Peralta and G. E. Scuseria, *Nano Lett.*, 2007, **7**, 2295.
59 E. J. Kan, Z. Y. Li, J. L. Yang and J. G. Hou, *J. Am. Chem. Soc.*, 2008, **130**, 4224.
60 M. H. Wu, Y. Pei and X. C. Zeng, *J. Am. Chem. Soc.*, 2010, **132**, 5554.
61 D. V. Kosynkin, A. L. Higginbotham, A. Sinitskii, J. R. Lomeda, A. Dimiev, B. K. Price and J. M. Tour, *Nature*, 2009, **458**, 872.
62 V. Barone, O. Hod and G. E. Scuseria, *Nano Lett.*, 2006, **6**, 2748.
63 D. Gunlycke, J. W. Li, J. W. Mintmire and C. T. White, *Nano Lett.*, 2010, **10**, 3638.
64 J. Li, Z. H. Zhang, D. Wang, Z. Zhu, Z. Q. Fan, G. P. Tang and X. Q. Deng, *Carbon*, 2014, **69**, 142.
65 Ž. Šljivančanin, *Phys. Rev. B: Condens. Matter Mater. Phys.*, 2011, **84**, 085421.
66 K. W. Lee and C. E. Lee, *Adv. Mater.*, 2012, **24**, 2019.

67 Y.-W. Son, M. L. Cohen and S. G. Louie, *Nature*, 2006, **444**, 347.
68 M. Brandbyge, J.-L. Mozos, P. Ordejón, J. Taylor and K. Stokbro, *Phys. Rev. B: Condens. Matter Mater. Phys.*, 2002, **65**, 165401.
69 J. M. Soler, E. Artacho, J. D. Gale, A. García, J. Junquera, P. Ordejón and D. Sánchez-Portal, *J. Phys.: Condens. Matter*, 2002, **14**, 2745.
70 P. Ayala, R. Arenal, A. Loiseau, A. Rubio and T. Pichler, *Rev. Mod. Phys.*, 2010, **82**, 1843.
71 L. J. Ci, L. Song, C. H. Jin, D. Jariwala, D. X. Wu, Y. J. Li, A. Srivastava, Z. F. Wang, K. Storr, L. Balicas, F. Liu and P. M. Ajayan, *Nat. Mater.*, 2010, **9**, 430.
72 L. Song, L. Balicas, D. J. Mowbray, R. B. Capaz, K. Storr, L. J. Ci, D. Jariwala, S. Kurth, S. G. Louie, A. Rubio and P. M. Ajayan, *Phys. Rev. B: Condens. Matter Mater. Phys.*, 2012, **86**, 075429.
73 J. P. Perdew, K. Burke and M. Ernzerhof, *Phys. Rev. Lett.*, 1996, **77**, 3865.
74 D. R. Kauffman, D. C. Sorescu, D. P. Schofield, B. L. Allen, K. D. Jordan and A. Star, *Nano Lett.*, 2010, **10**, 958.
75 Q. M. Yan, B. Huang, J. Yu, F. W. Zheng, J. Zang, J. Wu, B. L. Gu, F. Liu and W. H. Duan, *Nano Lett.*, 2007, **7**, 1469.
76 J. C. Dong and H. Li, *J. Phys. Chem. C*, 2012, **116**, 17259.
77 E. Lyyamperumal, S. Y. Wang and L. M. Dai, *ACS Nano*, 2012, **6**, 5259.
78 L. Pauling, *J. Am. Chem. Soc.*, 1932, **54**, 3570.
79 D. Gunlycke, J. W. Li, J. W. Mintmire and C. T. White, *Nano Lett.*, 2010, **10**, 3638.
80 F. W. Averill, J. R. Morris and V. R. Cooper, *Phys. Rev. B: Condens. Matter Mater. Phys.*, 2009, **80**, 195411.
81 X. J. Zhou, J. Y. Park, S. M. Huang, J. Liu and P. L. McEuen, *Phys. Rev. Lett.*, 2005, **95**, 146805.